


Role of CNTs on the Resistance to Delamination Growth in Three-Phase FRP Laminates with Embedded Delamination: Finite Element Analysis

Chukka Atchuta Rao¹ · K. S. R. K. Murthy¹ ·
D. Chakraborty¹ 

Received: 18 July 2023 / Accepted: 25 October 2023 / Published online: 2 December 2023
© The Institution of Engineers (India) 2023

Abstract The present work aims to investigate the effect of adding carbon nanotubes (CNTs) to epoxy on enhancing the resistance to growth of an existing embedded delamination in post-impact loading in a carbon/CNT + epoxy laminate. 3D finite element analyses are performed to determine the interlaminar stresses and strain energy release rate components at the elliptical delamination front which is elliptical using Irwin's crack closure integral. Results show that a significant increase in resistance to growth of embedded elliptical delamination could be achieved by mixing CNTs to epoxy limited to a specific weight percentage of CNTs only.

Keywords Three-phase composites · Carbon nanotube · Delamination · SERR · FEA

Introduction

Embedded interface delaminations caused due to low velocity impact, many a times go unnoticed and are the reasons for failure of FRP composite laminates in post-impact loading. In post-impact loading, such delaminations progress further and when a substantial area of the interface gets delaminated, the laminate fails catastrophically. There have been a good number of works reported on delamination damages due to low velocity impact and the influences of different factors on such delamination. Even though delamination induced due to accidental low velocity impact

may be over a very small area and might not immediately cause failure of the laminate, this may grow under post-impact routine load leading to failure. Therefore, it is also equally important to address the possibilities of improving resistance to delamination propagation from the existing delamination. Carbon/(CNT + epoxy) composites, where carbon fibers are reinforced in a matrix modified by adding CNTs in epoxy, are eyeing greater applications in aerospace, marine, armor and automotive industries because of their improved properties like enhanced strength and stiffness [1–3].

There have been a number of studies reported addressing how CNT wt% affects the CNT/polymer composite properties. Qiu et al. [4] conducted tensile and shear tests and results showed that the addition of 1 wt% of MWCNTs to epoxy led to an increase in tensile strength, modulus of elasticity and interlaminar shear strength (ILSS) by 14%, 20% and 5%, respectively. Experiments were conducted on carbon/epoxy laminates by Sharma and Shukla [5] and results revealed the enhancement of interlaminar shear strength, flexural modulus and Young's modulus by 40%, 38% and 51%, respectively, by the addition of just 1 wt% of CNT. Jain et al. [6] mixed CNTs in epoxy to prepare multiscale CFRP composite laminates and experimental results show an improvement of 17% and 28% in ultimate tensile strength and interlaminar shear strength, respectively, with 0.3 wt% of CNTs. Using FEA, Li et al. [7] reported that voids had a larger influence on transverse tensile properties than that on longitudinal tensile properties for CFRP composites.

Troung and Choi [8] added COOH-functionalized short MWCNTs in epoxy resin of woven CFRP composite laminates and results from the experiments confirmed that adding 0.5, 1 and 1.5 wt% of MWCNT, mode-I critical SERR (G_{Ic}) was enhanced by 1.6%, 31% and 31.7%,

✉ D. Chakraborty
chakra@iitg.ac.in

¹ Mechanical Engineering Department, IIT Guwahati,
Guwahati 781039, India

respectively. Romhany et al. [9] fabricated a 10-ply unidirectional multiscale CFRP laminate and experimental results confirmed that by adding 0.3 wt% non-functionalized MWCNTs, average fracture toughness could be improved by 13% in comparison with that of neat specimens. Burkov and Eremin [10] fabricated unidirectional CFRP composite laminates by modifying the resin with SWCNTs in the range of 0.1–0.5 wt% and their results revealed that with the addition of SWCNTs, while mode-I interlaminar fracture toughness showed a negative effect, mode-II interlaminar fracture toughness increased by 35%. Chavan et al. [11] introduced the nylon 6,6 nanofibers (1gm) at the interface of the E-glass fiber reinforced composites and experimental results showed an improvement of 24%, 30% and 40% in G_{IC} for 1.2 μm , 445 nm and 81 nm nanofiber diameters, respectively.

Delamination due to low velocity impact in fiber reinforced composites being an important research area, a large number of works have been reported where strain energy release rate (SERR) components are used to study the interface delamination and its propagation around the delamination front using the concepts of linear elastic fracture mechanics (LEFM). Hong and Liu [12] reported the delamination area or impact energy to be approximately the same as the critical SERR at the delamination front in low velocity impact justifying the use of SERR to compute the interlaminar fracture toughness. Finite element method has been extensively used for assessing delamination growth. Lu and Liu [13] computed the SERR around the circular delamination front by performing a full 3D finite element analysis and reported that the SERR components at the interface depend on the shape of the delamination, laminate thickness and the ply orientation of the adjacent ply.

Stress state ahead of the interfacial delamination is fully 3D and complex and it may not be easy to conduct experiments to understand the post-impact behavior in such cases and finite element analysis along with the concepts of fracture mechanics could be used advantageously to estimate the severity of delamination growth in such cases.

There have been a number of studies available on simulating the progressive damage in laminated composites using CZM as well as VCCT [14]. In CZM, the critical SERR needs to be known to capture delamination initiation and propagation. It is reported that the modeling effort and the required computational time are much higher in the CZM approach, the VCCT and CZM approach provides a similar prediction of delamination at the interface [15]. Therefore, VCCT method could be advantageously used when deciding the SERR components as well as critical SERR for estimating the resistance to the growth of interfacial delamination. On the other hand, the stress-based criteria are also used for assessing delamination [16–18] using the interactions among the interlaminar

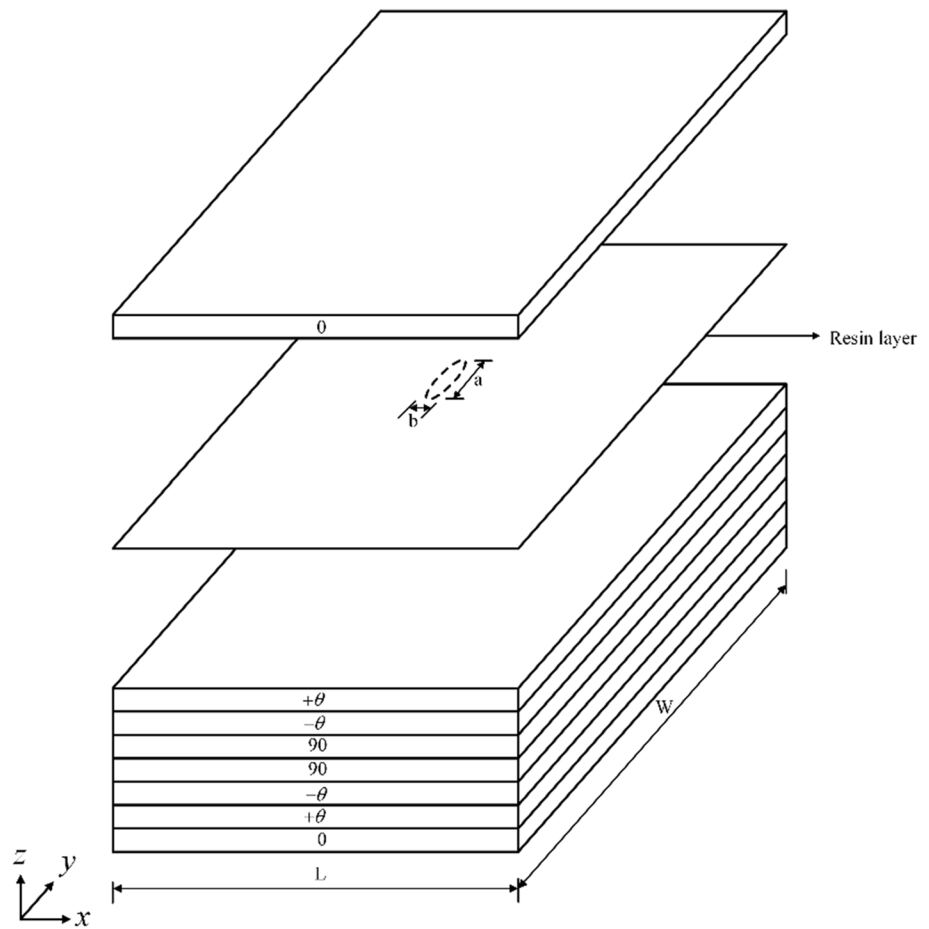
stresses and the corresponding strengths. However, not much data are available regarding the critical SERR as well as the interlaminar strengths of laminates, especially when the matrix is modified by adding CNTs. It has already been reported that the modified matrix (CNT + epoxy) shows brittle fracture [10], and therefore, the concepts of LEFM could be advantageously used to analyze such composites. Whereas, simple micromechanics models could be used to estimate the effective properties of CNT + epoxy [19] which could be used to assess the delamination initiation and propagation using stress-based approach but the same is not well understood for determination of effective fracture properties like SERR. Thus, a combined stress-based and fracture mechanics-based approach was thought of in assessing the critical SERR to decide the role of CNTs in enhancing the resistance to propagation of delamination caused due to low velocity impact in the post-impact loading.

Even though there have been a good number of works available on the simulation of delamination propagation using VCCI as well as CZM, no work has been reported on the study of the effect of mixing CNTs to the epoxy in enhancing the resistance to growth of an existing subsurface delamination. In addition, the fact that growth of such delamination is a complex phenomenon and is difficult to conduct experiments, it is important that an FE-based estimate of role of CNTs in possible enhancement of the resistance to further growth of such delamination is understood. Therefore, the objective of this work is to understand the quantitative and qualitative influence of adding CNTs to epoxy in resisting further growth from an embedded elliptical delamination caused by low velocity impact in the post-impact loading. Here, a combination of stress-based criterion and VCCI has been used along with a 3D FE to assess the potential growth of an existing embedded delamination and then study the role of mixing CNTs with epoxy on such growth.

FE Analysis of Delamination: Stresses and SERR

Delamination is the separation of the adjacent lamina at the interface of laminated composites and the interlaminar stresses σ_{zz} , τ_{xz} and τ_{yz} (Fig. 1) are responsible for such delamination. Therefore, to assess delamination at the interface, a complete 3D stress analysis is required. In addition, the stresses are singular at the delamination front; hence, fracture mechanics can be used to study delamination propagation using parameters like SERR. Delamination may initiate at the free edges of the laminate or when a laminated specimen experiences a low velocity impact, delamination usually occurs at a specific interface below the impact site as shown in Fig. 1. At the interface,

Fig. 1 Exploded view of a laminate having an embedded delamination



such delamination progresses in a resin layer which is thin and is located between two adjacent laminae.

Delamination propagation could be estimated by two approaches, viz. strength of materials approach and the fracture mechanics approach. In strength of materials approach, propagation of delamination is assessed by comparing the local state of stress with the relevant strengths, whereas SERR is evaluated in the fracture mechanics approach and compared with critical SERR. Earlier researchers have proposed many criteria for estimating delamination initiation and among those, an extensively used one is the quadratic stress criterion (QSC) [16], which indicates that the condition given by Eq. (1) needs to be satisfied for delamination initiation.

$$Q \left(= \left[\frac{\bar{\sigma}_{zz}}{Z} \right]^2 + \left[\frac{\bar{\tau}_{xz}}{X} \right]^2 + \left[\frac{\bar{\tau}_{yz}}{Y} \right]^2 \right) \geq 1 \tag{1}$$

where $\bar{\sigma}_z$, $\bar{\tau}_{xz}$, $\bar{\tau}_{yz}$ are the average stresses (refer Fig. 1) computed along a very small length (Δa) measured from the delamination front given by

$$\bar{\sigma}_{zz} = \frac{1}{\Delta a} \int_0^{\Delta a} \sigma_{zz} dx \tag{2}$$

$$\bar{\tau}_{xz} = \frac{1}{\Delta a} \int_0^{\Delta a} \tau_{xz} dx \tag{3}$$

$$\bar{\tau}_{yz} = \frac{1}{\Delta a} \int_0^{\Delta a} \tau_{yz} dx \tag{4}$$

and X, Y and Z represent the corresponding interlaminar shear strengths and interlaminar normal strength, respectively. In applying QSC, the length (Δa) over which the stresses are averaged generally depends on the type of the laminate and the dimension and is generally very small [16] as the maximum stress at the interface exists over only a very small length ahead of the singular point. In this work, a very small $\Delta a = 0.05$ mm has been decided after conducting number of numerical experimentation starting from $\Delta a = 0.5$ mm and successively reducing Δa

till the average interlaminar stresses at the interface at the delamination front converges.

Kruger et al. [20] assessed the initiation of delamination at the interface with the help of virtual crack closure integral (VCCI), where the components of SERR are evaluated and compared with the respective critical SERRs. The elliptical delamination considered here has a curved delamination front as shown in Fig. 2. In order to calculate SERR components on the curved delamination front, the transformation of coordinates on stresses and displacements is performed. A 3D finite element analysis is performed to evaluate σ_{zz} , τ_{zn} , τ_{zt} (interlaminar stresses) and the corresponding displacements. The SERR components, G_I , G_{II} , and G_{III} at a point (P in Fig. 2) on the curved delamination front have been computed using the following equations:

$$G_I = \lim_{\Delta a \rightarrow 0} \frac{1}{2c\Delta a} \int_0^{\Delta a} \int_0^c \sigma_{zz} \delta u_z(n - \Delta a) \, dn \, dt \quad (5)$$

$$G_{II} = \lim_{\Delta a \rightarrow 0} \frac{1}{2c\Delta a} \int_0^{\Delta a} \int_0^c \tau_{zn} \delta u_n(n - \Delta a) \, dn \, dt \quad (6)$$

$$G_{III} = \lim_{\Delta a \rightarrow 0} \frac{1}{2c\Delta a} \int_0^{\Delta a} \int_0^c \tau_{zt} \delta u_t(n - \Delta a) \, dn \, dt \quad (7)$$

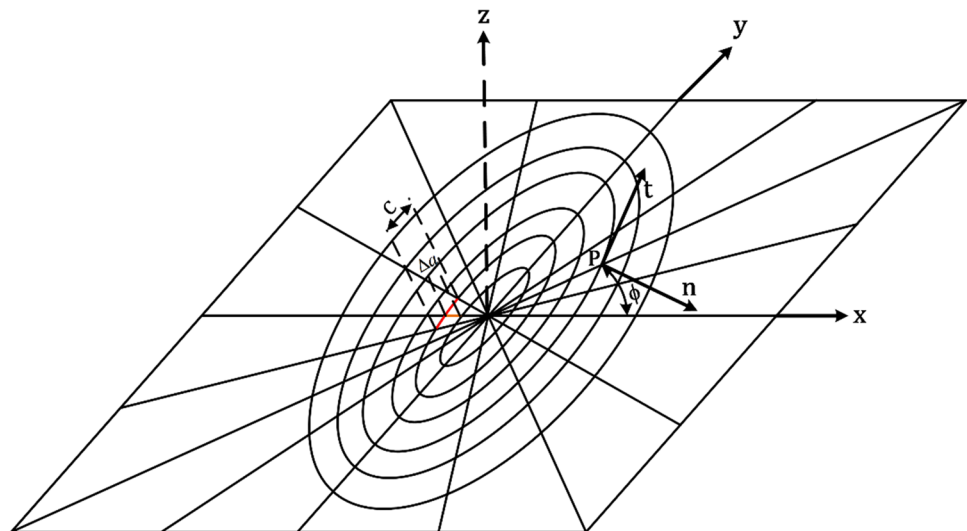
Referring to Fig. 2, at a point P on the delamination front, n is the normal and t is the tangent. Δa is the virtual crack extension length along the direction n . δu_n is the relative displacement of top and bottom surface at a point Δa behind the delamination front along n . δu_t and δu_z are the relative displacements of top and bottom surface at that point along the tangential direction (along t) and along z (normal

to n and t), respectively. σ_z , τ_{zn} and τ_{zt} are interlaminar stresses at the interface needed to close the crack. The total SERR for a small delamination length can be calculated as $G = G_I + G_{II} + G_{III}$. At the interface, critical SERR has been evaluated using QSC in conjunction with VCCI. Delamination initiation is predicted using QSC (Eq. (1)). At the instant where delamination initiation has been predicted by the QSC, components of SERR are calculated using VCCI (Eqs. (5)–(7)) and the total SERR at that instant is the critical SERR (G_c) as satisfying the condition, $G \geq G_c$ results in delamination initiation.

Geometry of the Specimen and Material Properties

As shown in Fig. 1, a laminated composite specimen having embedded delamination is considered. It is reported that under low velocity impact delamination occurs at the interface and is generally in the shape of peanut which is approximately equal to ellipse. Therefore, in this case, a square $[0/\pm\theta/90]_s$ laminate is considered and $[0/+ \theta]$ the interface is modeled by inserting a thin layer of resin containing an elliptical delamination as shown in Fig. 1. The laminated specimen is of 100 mm length (L), 100 mm wide (W) and the ply thickness is 0.127 mm. The embedded elliptical delamination has a major axis $a=2$ mm, and a minor axis $b=1$ mm and the eccentricity of delamination is $e=a/b=2$. The laminate is considered to be made of carbon/(CNT + epoxy) laminate with 60% fiber volume fraction and carries an axial tension. The laminae properties are evaluated by first computing the properties of the matrix (CNT + epoxy) with the help of Halpin–Tsai relations [19]. Next, the carbon/(CNT + epoxy) composite properties are evaluated using the rule of mixtures. For

Fig. 2 Elliptical delamination front



composites in which CNTs are considered to be randomly oriented and uniformly distributed throughout the resin matrix, the Halpin–Tsai equations are more elaborate and correlate specific geometric characteristics of CNTs, and the relative modulus of elasticity of a composite is related to the properties of the individual constituents by the following equation

$$E_c = \left(\frac{3}{8} \frac{1 + \zeta \eta_L V_{CNT}}{1 - \eta_L V_{CNT}} + \frac{5}{8} \frac{1 + 2\eta_T V_{CNT}}{1 - \eta_T V_{CNT}} \right) E_m \tag{8}$$

where $\zeta = 2l/d$, η_L and η_T are the parameters which are represented by

$$\eta_L = \frac{(E_{CNT}/E_m) - 1}{(E_{CNT}/E_m) + (2l/d)} \tag{9}$$

$$\eta_T = \frac{(E_{CNT}/E_m) - 1}{(E_{CNT}/E_m) + 2} \tag{10}$$

where E_c = elastic modulus of the CNT + epoxy, E_{CNT} = elastic modulus of CNTs = 400 GPa, E_m = elastic modulus of neat epoxy = 3.1 GPa, l = length of CNTs = 30 μm , d = diameter of CNTs = 20 nm, t = thickness of graphite layer used to make CNTs = 3.4 \AA , and V_{CNT} = volume fraction of CNTs given by the following equation

$$V_{CNT} = \frac{1}{[(\rho_{CNT}/\rho_m) \times (M_m/M_{CNT})] + 1} \tag{11}$$

where ρ_{CNT} = density of CNTs = 2.1 g/cc, ρ_m = density of epoxy matrix = 1.2 g/cc, M_m is the mass fraction of epoxy matrix, and M_{CNT} is the mass fraction of CNTs. As the mass fraction of CNTs is small, Poisson’s ratios of the epoxy and CNT composite were considered to be the same. The shear modulus for the matrix (CNT + epoxy) is calculated as

$$G_{\text{comp}} = \frac{E_c}{2(1 + \nu)} \tag{12}$$

Generally, adding CNTs to a resin matrix can improve the material’s mechanical, electrical and thermal properties. However, adding too much CNTs may adversely affect material properties due to poor dispersion and aggregation of the CNTs within the matrix. The optimum weight percent of CNTs in a resin matrix typically ranges from 0.1% to 5%, though the exact amount may vary depending on the specific resin matrix and CNTs used. Hence, in the present study a range of 0–1.5 wt% is considered for the analysis.

Mechanical properties of the CNT + epoxy and the carbon/CNT + epoxy composite for different wt% (0, 0.25, 0.5, 1 and 1.5) of CNTs following the above discussion are calculated and are presented in Tables 1 and 2, respectively. The laminae are considered as transversely isotropic material

Table 1 CNT+epoxy properties

CNT wt%	(CNT+epoxy)		
	Tensile modulus (GPa)	Poisson’s ratio	Shear modulus (GPa)
0.0%	3.10	0.35	1.15
0.25%	3.31	0.35	1.23
0.50%	3.53	0.35	1.31
1.00%	3.95	0.35	1.46
1.50%	4.38	0.35	1.62

and the five elastic constants corresponding to different CNT wt% are shown in Table 2. It may be noted from Table 2 that adding CNTs to the epoxy resulted in a substantial improvement in the tensile modulus and shear modulus. Adding 1.5 wt% of CNTs to the epoxy resulted in a 41% increase in tensile modulus and a 40% increase in the shear modulus of the matrix. However, when this CNT + epoxy is used as the matrix in the carbon/(CNT + epoxy) lamina, an increase of 40% in transverse tensile modulus and 38% in shear modulus (in-plane) was observed but the increase in longitudinal tensile modulus is insignificant. This is due to the fact that the tensile modulus of carbon fiber is much higher than that of the matrix.

Interlaminar shear strengths (X and Y) for different CNT wt% are taken from [5] where short beam shear tests were conducted to estimate the ILSS. Normal cohesive strength (NCS) experiments have been conducted on composites [21] and it was reported that the interlaminar normal strength is approximately half of the interlaminar shear strength. Hence, in the present case, ILNS is considered half the magnitude of ILSS. The values of X, Y and Z for different wt% of CNTs are shown in Table 3.

Results and Discussions

Interlaminar stresses at the delamination fronts are computed for different configurations of laminate using the 3D FE analysis. Also, the components of SERR are computed to understand the effect of adding CNTs to the epoxy on the propensity of the delamination to grow further under loading.

Finite Element Modeling

The carbon/(CNT + epoxy) laminate having an interfacial delamination of elliptical shape has been analyzed using 3D FEA in ANSYS Mechanical APDL (ANSYS 22). From the 3D FEA, interlaminar stresses and displacements are evaluated, and SERRs were computed using virtual crack

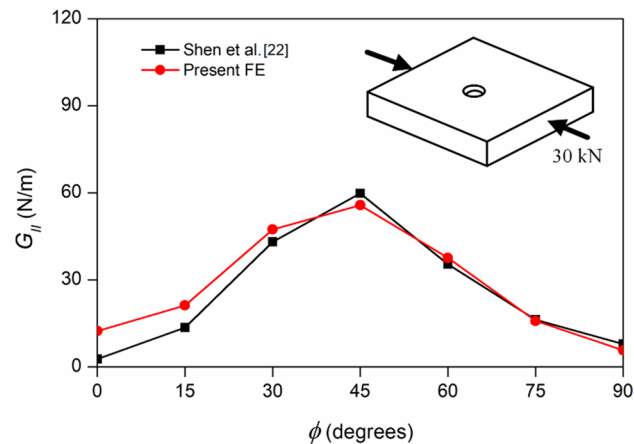
Table 2 Elastic properties carbon/(CNT + epoxy) composites

CNT wt%	E_1 (GPa)	$E_2=E_3$ (GPa)	$G_{12}=G_{13}$ (GPa)	G_{23} (GPa)	$\nu_{12}=\nu_{13}$	ν_{23}
0.0%	139.24	7.59	2.75	3.63	0.284	0.045
0.25%	139.33	8.11	2.93	3.86	0.284	0.051
0.50%	139.41	8.62	3.11	4.08	0.284	0.056
1.00%	139.58	9.63	3.46	4.53	0.284	0.063
1.50%	139.75	10.65	3.81	4.96	0.284	0.073

1–2: Longitudinal and transverse (in-plane) directions; 3: Out-of-plane direction

Table 3 Interlaminar shear and normal strengths [5, 21]

CNT wt%	X (MPa)	Y (MPa)	Z (MPa)
0.0%	35	35	17
0.25%	41	41	20
0.50%	43	43	22
1.00%	48	48	24
1.50%	47	47	23

**Fig. 3** G_{II} around a circular delamination front

integration technique. However, the VCCI-based evaluation of SERR has been first validated before using the same for analysis of the embedded delamination to ensure that the SERR components are accurately calculated with appropriate mesh refinement.

Validation

To validate the computed SERR around a circular delamination front, using the present FE analysis and virtual crack closure integral, a $[(0/+45/-45)_3]_s$ square laminate with a side of 50 mm, and a centrally located through hole of 5 mm in diameter, is considered following the work of Shen et al. [22]. Mode II SERR determined using VCCI in the present FEA is compared with that of Shen et al. [22]

and a good qualitative and quantitative agreement could be seen as shown in Fig. 3.

FEA of the Laminate with an Embedded Delamination

In the present FEA, the three-phase FRP laminate specimen has been modeled as three distinct layers, viz. the top and bottom sub-laminates as two layers and a thin resin-rich layer (thickness = 0.1 times the ply thickness) representing the interface. Modeling the interface with a resin-rich layer is justified by the fact that delamination in FRP laminated composites actually progresses in a thin resin layer at the interface of the adjacent laminae [23]. In addition, it has been also reported that in the case of laminated FRP composites, the stress singularity which is oscillatory at the interface could be eliminated by introducing a very thin resin-rich layer [24]. SOLID 185 elements from ANSYS element library (three-dimensional, eight-noded, layered) are used for discretizing the laminate having an embedded delamination at the interface, and layer-wise orthotropic properties have been input.

It is reported [25] that the FEA solutions might lead to inaccurate results due to delaminated layers interpenetrating each other and hence in the present FEA, the bottom and the top nodes of the delaminated region are connected through bilinear contact element (CONTA 178) ensuring no interpenetration of delaminated layers. The resin-rich interface has been modeled by providing the isotropic properties of resin (CNT + epoxy) as input and the elliptical delamination has been modeled by deleting elements from the resin layer. Figure 4a, b shows the full 3D FE mesh of a square laminate and zoomed view of mesh near embedded elliptical delamination, respectively. The axial loading of the laminate is simulated by fixing one edge of the laminate and the opposite edge is subjected to axial displacement ($\epsilon = 0.005$) as shown in Fig. 4a.

In order to capture the stiff stress gradient at the delamination front, a very fine mesh is used near the delamination front. Table 4 shows the convergence of interlaminar shear stress with progressive mesh refinement. In the present case, the mesh convergence has been attained with 37,632 number of elements near the delamination front as shown in Fig. 5. Different values of the eccentricity of the

Fig. 4 **a** FE mesh of square laminate and **b** zoomed mesh near embedded elliptical delamination

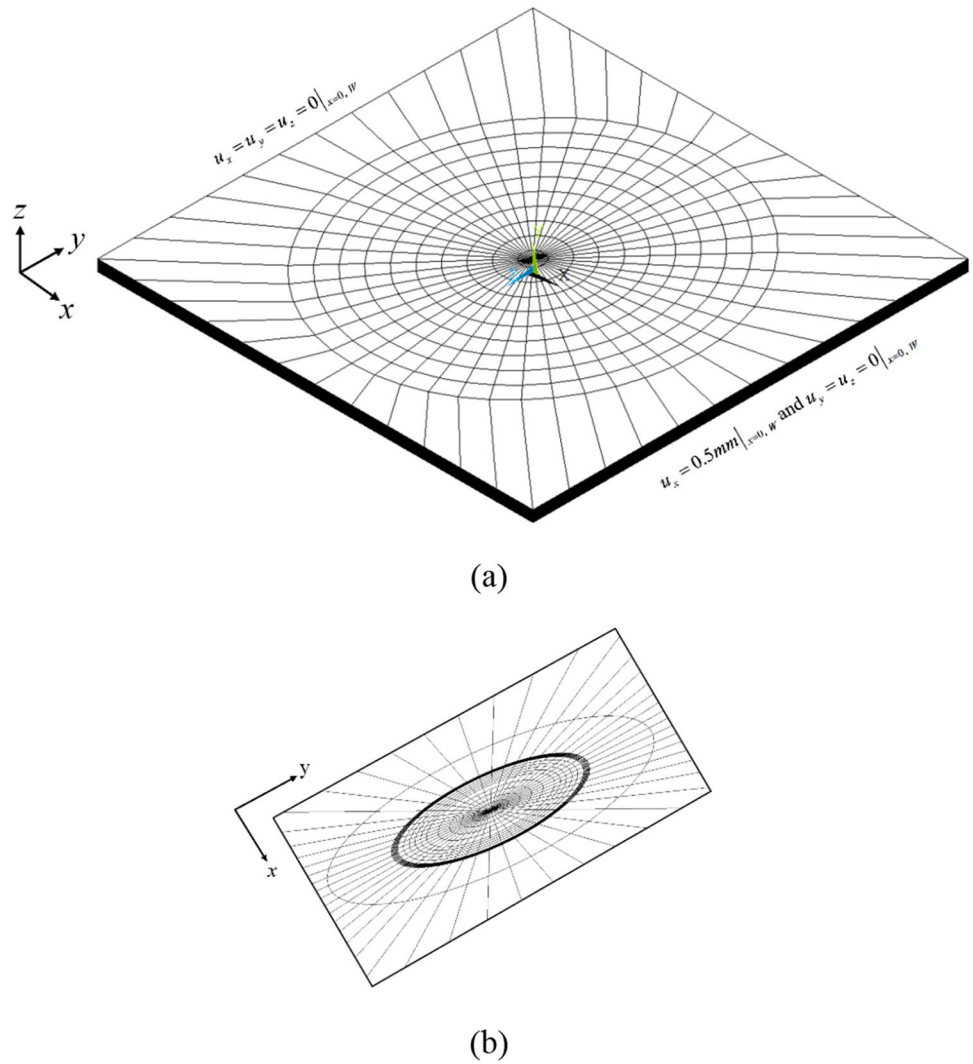


Table 4 FE mesh convergence

Mesh number	Total number of elements	τ_{zn} (MPa)
1	10,752	20.3
2	16,128	21.9
3	21,504	22.8
4	26,880	23.3
5	32,256	23.9
6	37,632	23.8
7	43,008	23.8

embedded elliptical delamination have been considered to understand the effect of the delamination shape.

Interlaminar Stresses along the Delamination Front

Even though the laminate is loaded axially, due to centrally located embedded delamination at the interface, in-plane,

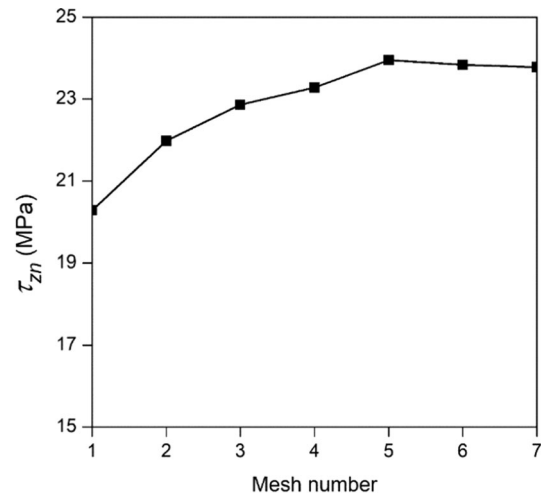


Fig. 5 Convergence of FE mesh for carbon/epoxy composite

as well as out-of-plane stresses are observed along the delamination. Using the 3D FEA, considering the delamination front near the elliptical delamination as the crack, the interlaminar stresses at the interface are computed using Eqs. (2–4).

Variation of interlaminar stresses σ_z , τ_{zn} and τ_{zt} are shown in in Fig. 6a–c, respectively, along the delamination front (represented by angle measured from to x-axis) for a $[0/\pm\theta/90]_s$ carbon/epoxy laminate having an embedded delamination for $\theta = 0^\circ$. All these stresses are average stresses measured over a very small distance in front of the delamination. Stress variation along half of the total delamination front ($0^\circ - 180^\circ$) has been shown since the variation is symmetric. Existence of all the three out-of-plane components of stresses in the delamination front clearly shows a 3D state of stress at the delamination front. Thus, it could be inferred that the delamination at the

interface will be mixed-mode even though the applied load is purely axial.

Strain Energy Release Rate along the Delamination Front

From the FE analysis, required interlaminar stresses and nodal displacements are computed to calculate SERR components at the delamination front using VCCI (Eqs. 5–7) and are plotted around the delamination front (angular location with reference to x-axis).

Figure 7a–c shows the variation of G_I , G_{II} and G_{III} , respectively, around the delamination front for $e = 1$ and $\theta = 0^\circ$ degrees. It could be observed that in accordance with the variation of interlaminar stresses, the components of SERR also vary following a similar trend around the delamination front. However, it could be noted that the

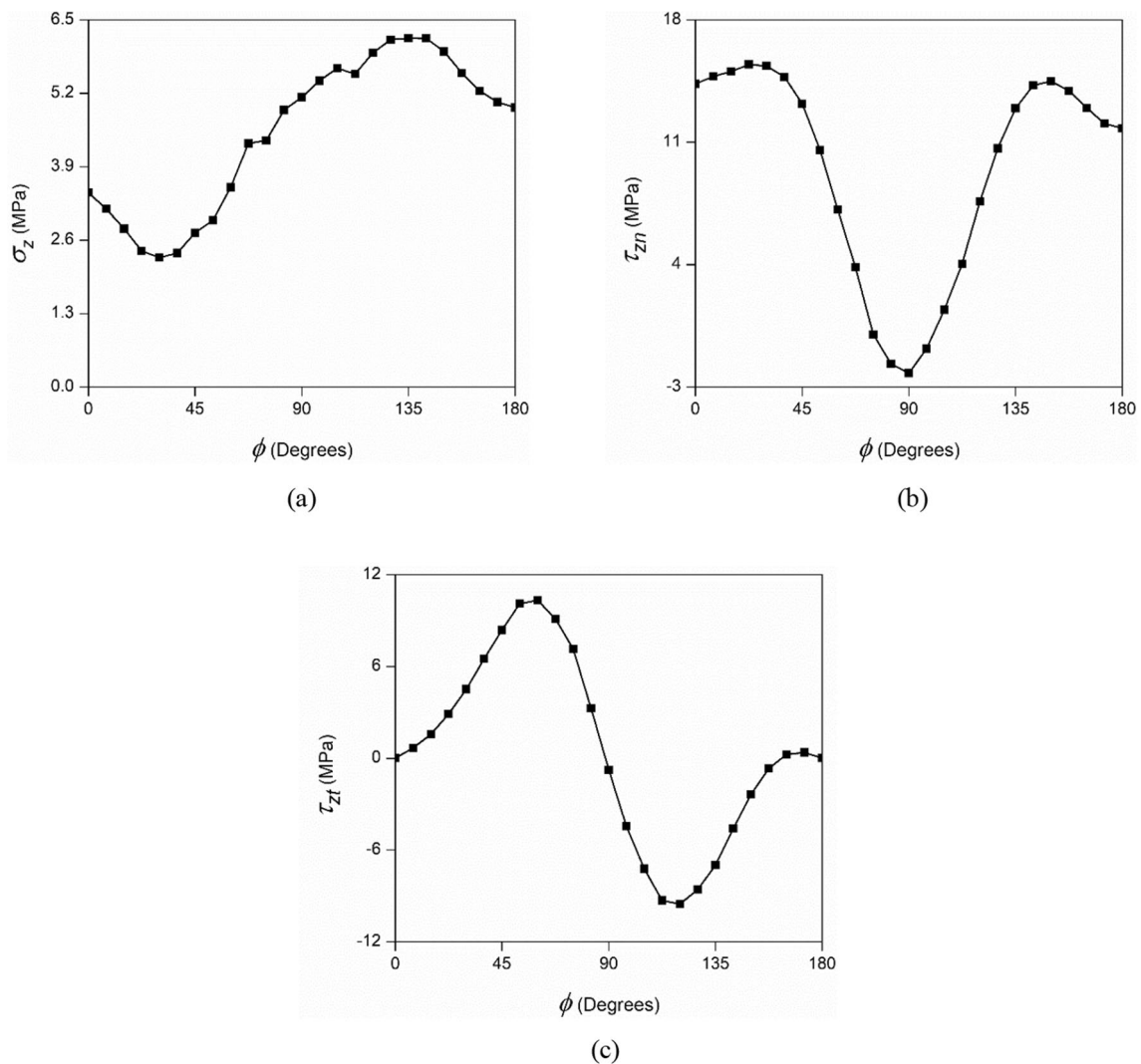


Fig. 6 Variation of **a** σ_z , **b** τ_{zn} and **c** τ_{zt} along the delamination front

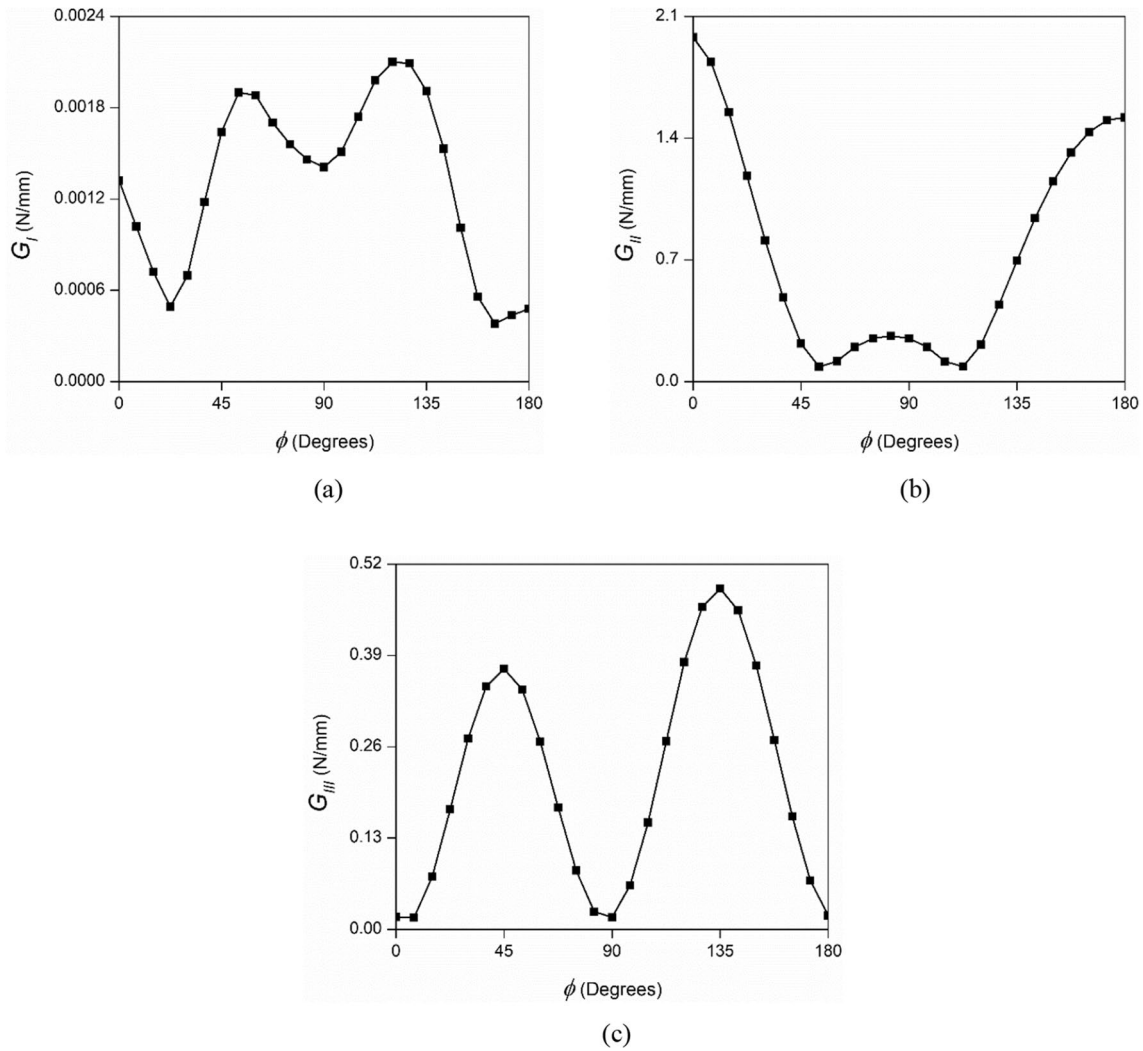


Fig. 7 Variation of a G_I , b G_{II} and c G_{III} along the delamination front

magnitude of G_I is much smaller compared to those of G_{II} and G_{III} , showing that mode II and mode III dominate. Similar to the stress variation, the maximum magnitude of SERR components also occur at different locations, showing that it is the combination of G_I , G_{II} and G_{III} that will decide whether the delamination will grow further or not. In the present case, G_{II} is maximum at $\phi=0^\circ$ and G_{III} is maximum at $\phi=135^\circ$. The same trend has also been obtained for different aspect ratios of the delamination; however, the magnitudes of G_{II} and G_{III} are different.

Effect Delamination Shape

To understand how the delamination shape at the interface influences the SERR, the delamination shape ($e = a/b$) is varied from 1 to 2.5 and SERRs are computed using VCCI along the delamination front.

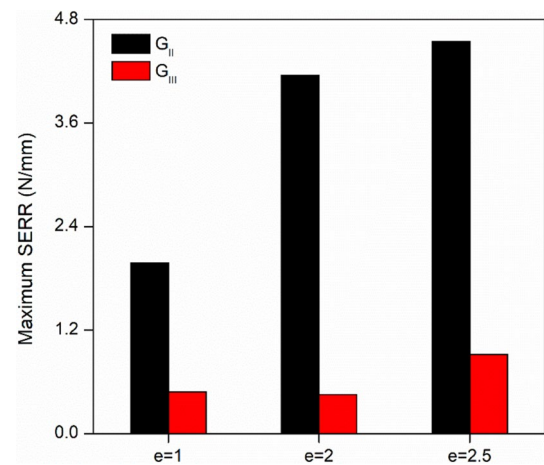


Fig. 8 Maximum SERR for different aspect ratios of the delamination

Figure 8 shows the variation of maximum magnitudes of G_{II} and G_{III} with increasing aspect ratio, $e (=a/b)$ for $\theta = 0^\circ$ degrees. In the present case, with the increase in e , there is a substantial increase in both $G_{II\max}$ and $G_{III\max}$ showing that the chances of further growth along the delamination front increase with the increase in aspect ratio.

Effect of Fiber Orientation

In order to understand how the relative fiber orientation of the adjacent laminae at the interface affects the SERR components, the fiber orientation angle (θ) of the adjacent lamina is varied from 0° to 90° . From the previous Sect. it has been observed that SERR is maximum for an aspect ratio of 2.5. Hence, in the present case, SERR is computed for $e = 2.5$ using Eqs. 5–7.

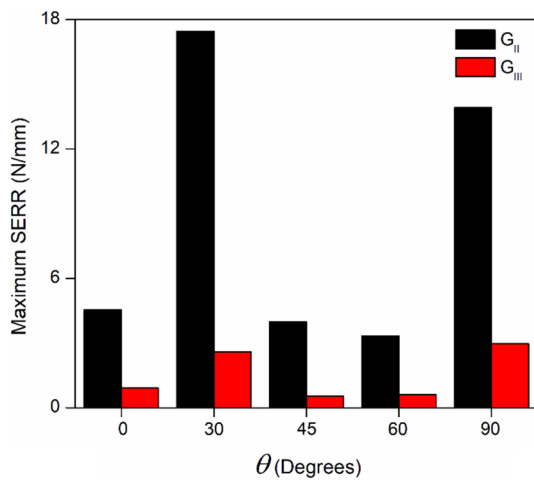


Fig. 9 Maximum SERR for different fiber orientations ($e = 2.5$)

Figure 9 shows the variation of $G_{II\max}$ and $G_{III\max}$ along the delamination fronts with the fiber orientation angle θ . It has been observed that $G_{II\max}$ is maximum for $\theta = 30^\circ$ and $G_{III\max}$ is maximum for $\theta = 90^\circ$ though the magnitude of $G_{II\max}$ is much higher compared to that of $G_{III\max}$. The reason for $G_{II\max}$ to be maximum for $\theta = 30^\circ$ is because the property mismatch causing τ_{zn} is maximum corresponding to $0^\circ/30^\circ$ interface. Similarly, the reason for $G_{III\max}$ to be maximum for $\theta = 90^\circ$ is because the property mismatch causing τ_{zt} is maximum corresponding to $0^\circ/90^\circ$ interface. Similar experimental results have been observed where SERR increases with the increase in fiber angle [26].

Effect of CNT wt% on SERR

To study the effect of CNT wt% on SERR components, different CNT wt% (0%, 0.25%, 0.5%, 1% and 1.5%) are considered, SERR are computed for different eccentricities and different fiber orientations.

Figure 10a, b shows the variation of $G_{II\max}$ and $G_{III\max}$, respectively, on the delamination front with increasing CNT wt%. Since G_{II} is maximum for $\theta = 30^\circ$, therefore variation in $G_{II\max}$ with CNT wt% is shown only for $\theta = 30^\circ$. Similarly, the variation of $G_{III\max}$ with CNT wt% is shown only for $\theta = 90^\circ$. In both the cases, variation is shown for $e = 2.5$. It could be observed that both $G_{II\max}$ and $G_{III\max}$ values show reduction with increasing CNT wt% in the epoxy. It has been observed that $G_{II\max}$ and $G_{III\max}$ values are reduced by 11% and 20%, respectively, compared to those for neat resin with the addition of 1.5 wt% CNTs in epoxy. This indicates that mixing CNTs with epoxy reduces the chances of interfacial delamination growing further from an existing embedded delamination. However, the value of critical SERR (G_c) decides whether

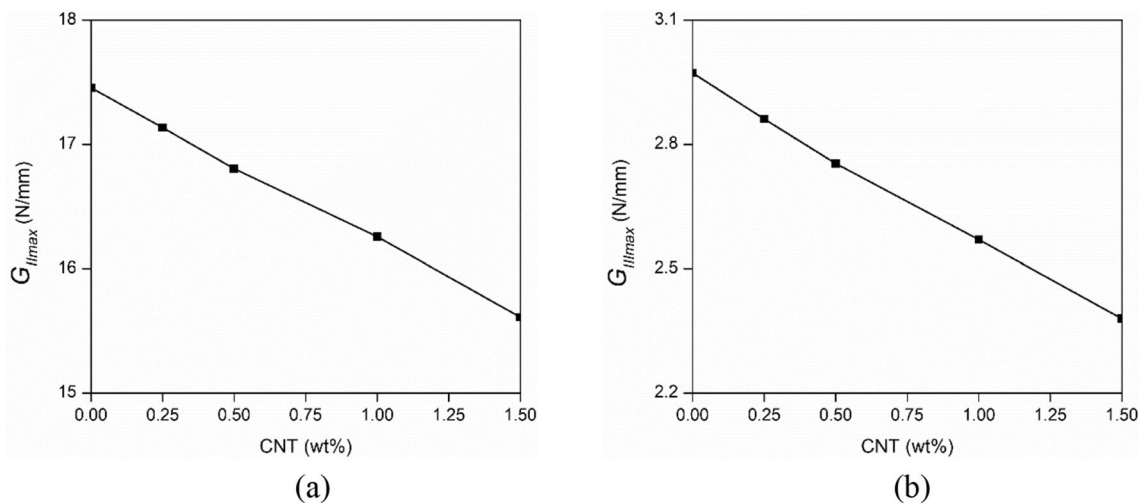


Fig. 10 Variation of a $G_{II\max}$ b $G_{III\max}$ with CNT wt% for $e = 2.5$

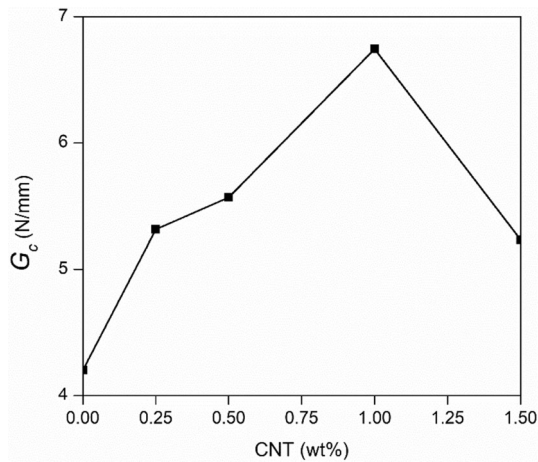


Fig. 11 Variation of G_c with CNT wt%

delamination will grow further or not, and thus it is essential to calculate G_c for the same laminate.

Critical SERR (G_c) and Influence of CNT wt%

Critical SERR (G_c) is used as a metric for resistance to delamination growth and the same has been computed using QSC and VCCI. In the present case, G_c has been calculated for different CNT wt% in CNT + epoxy to understand how mixing CNTs with epoxy actually enhances the resistance to the further growth of embedded delamination. Since the SERR is maximum corresponding to $e=2.5$ and for $\theta = 30^\circ$, therefore the variation of G_c with CNT wt% has been computed corresponding to $e=2.5$ and $\theta = 30^\circ$, and Fig. 11 shows the variation with different CNT wt%. It could be seen from Fig. 11 that as CNT wt% increases, the magnitude of G_c increases substantially and reaches a maximum at 1 wt%. However, with the further increase in CNT beyond 1 wt%, value of G_c decreases though still higher than that corresponding to the case of neat resin. This is due to the combined effect of change in stiffness and strength of the lamina with increasing CNT wt%. It could be observed that the corresponding to 1 wt% of CNT, increase in G_c is 65% more than that of neat resin. Therefore, it is inferred that mixing CNTs with epoxy results in significant enhancement in the resistance to further growth of delamination in the post-impact loading, but there is a limit to CNT wt% to which this enhancement is maximum which is 1% in the present case.

Similar experimental results [27] were also reported where it was shown that there is a considerable increase in laminate interface strength with an increase in carbon nanofillers up to a limited weight percent only.

Conclusions

The present work investigates the role of CNTs in a three-phase carbon/CNT + epoxy laminate on the resistance to post-impact delamination growth from an embedded elliptical delamination caused due to low velocity impact. Using VCCI- and stress-based criterion, 3D FEAs are carried out to calculate the critical SERR indicating the resistance to growth of delamination corresponding to different CNT wt% and the following important conclusions have been drawn.

1. Adding of CNTs to the epoxy results in substantial improvement in resistance to growth of delamination from an existing embedded delamination at the interface in post-impact loading.
2. The magnitudes of SERR components at the delamination front reduce due to mixing of CNTs to the epoxy indicating reduced chance for delamination to grow at the interface. In the present study, in the most severe case of delamination, the addition of 1.5 wt% CNTs in epoxy indicates a reduction of $G_{II\max}$ and $G_{III\max}$ values by 11% and 20%, respectively, compared to those for neat epoxy (without CNT).
3. Critical SERR (G_c), a metric to the delamination growth resistance, is significantly increased by the adding CNTs to epoxy. Present study shows that adding 1 wt% CNTs to the epoxy leads to a 65% increase in G_c of the carbon/(CNT + epoxy) laminate.
4. Addition of CNTs to epoxy though leads to significant enhancement in resistance to delamination growth, there is a limit beyond which further adding more of CNTs to epoxy results in a reduction in the resistance. Thus, in order to achieve maximum resistance to delamination growth at the interface from an embedded elliptical delamination, it is necessary to identify the optimum amount of CNT wt% to be added with the epoxy.

Author Contributions CAR was involved in conceptualization, programming, validation, draft preparation. KSRM and DC helped in conceptualization, review and editing.

Funding The authors have not been funded in any way to carry out the research activities.

Declarations

Competing interests The authors declare that they have no known competing financial interests or personal relationships that could have appeared to influence the work reported in this paper.

References

1. C.H. Tseng, C.C. Wang, C.Y. Chen, Functionalizing carbon nanotubes by plasma modification for the preparation of covalent-integrated epoxy composites. *Chem. Mater.* **19**(2), 308–315 (2007). <https://doi.org/10.1021/cm062277p>
2. A.T. Seyhan, M. Tanoglu, K. Schulte, Mode I and mode II fracture toughness of E-glass non-crimp fabric/carbon nanotube (CNT) modified polymer based composites. *Eng. Fract. Mech.* **75**(18), 5151–5162 (2008). <https://doi.org/10.1016/j.engfracmech.2008.08.003>
3. A. Dorigato, A. Pegoretti, F. Bondioli, M. Messori, Improving epoxy adhesives with zirconia nanoparticles. *Compos. Interfaces* **17**(9), 873–892 (2010). <https://doi.org/10.1163/092764410X539253>
4. J. Qiu, C. Zhang, B. Wang, R. Liang, Carbon nanotube integrated multifunctional multiscale composites. *Nanotechnology* **18**(27), 275708 (2007). <https://doi.org/10.1088/0957-4484/18/27/275708>
5. K. Sharma, M. Shukla, Three-phase carbon fiber amine functionalized carbon nanotubes epoxy composite: processing, characterisation, and multiscale modeling. *J. Nanomater.* (2014). <https://doi.org/10.1155/2014/837492>
6. V. Jain, S. Jaiswal, K. Dasgupta, D. Lahiri, Influence of carbon nanotube on interfacial and mechanical behavior of carbon fiber reinforced epoxy laminated composites. *Polym. Compos.* **43**(9), 6344–6354 (2022). <https://doi.org/10.1002/pc.26943>
7. Y. Li, L. Zhou, M. Zhang, C. Song, Study on the effect of void defect on mechanical properties of carbon fiber composites by finite element method. *J. Inst. Eng. India Ser. C* **103**, 1433–1446 (2022). <https://doi.org/10.1007/s40032-022-00881-1>
8. G.T. Troung, K.K. Choi, Effect of short multi-walled carbon nanotubes on the mode I fracture toughness of woven carbon fiber reinforced polymer composites. *Construct. Build. Mater.* **259**, 119696 (2020). <https://doi.org/10.1016/j.conbuildmat.2020.119696>
9. G. Romhányi, G. Szebényi, Interlaminar crack propagation in MWCNT/fiber reinforced hybrid composites. *Express Polym Lett* **3**(3), 145–151 (2009). <https://doi.org/10.3144/expresspolymlett.2009.19>
10. M. Burkov, A. Eremin, Evaluation of fracture toughness of hybrid CNT/CFRP composites. *Mech. Adv. Mater. Struct.* (2022). <https://doi.org/10.1080/15376494.2022.2064569>
11. S. Chavan, N.J. Kanu, S. Shendokar, B. Narkhede, M.K. Sinha, E. Gupta, G.K. Singh, U.K. Vates, An insight into nylon 6,6 nanofibers interleaved E-glass fiber reinforced epoxy composites. *J. Inst. Eng. India Ser. C.* **104**, 15–44 (2023). <https://doi.org/10.1007/s40032-022-00882-0>
12. S. Hong, D. Liu, On the relationship between impact energy and delamination area. *Exp. Mech.* **29**, 115–120 (1989). <https://doi.org/10.1007/BF02321362>
13. X. Lu, D. Liu, Finite element analysis of strain energy release rate at delamination front. *J. Reinf. Plast. Compos.* **10**(3), 279–292 (1991). <https://doi.org/10.1177/073168449101000303>
14. J. Jokinen, M. Kanerva, M. Wallin, O. Saarela, The simulation of a double cantilever beam test using the virtual crack closure technique with the cohesive zone modelling. *Int. J. Adhes. Adhes.* **88**, 50–58 (2019). <https://doi.org/10.1016/j.ijadhadh.2018.10.015>
15. B.R. Sindhu, J. Raju, K. Kamath, Comparative numerical study of standard 3D composite plate using virtual crack closure technique and cohesive zone modelling method. *IOP Conf. Ser. Mater. Sci. Eng.* **561**, 1–8 (2019). <https://doi.org/10.1088/1757-899X/561/1/012048>
16. J.C. Brewer, P.A. Lagace, Quadratic stress criterion for initiation of delamination. *J. Compos. Mater.* **22**(12), 1141–1155 (1988). <https://doi.org/10.1177/002199838802201205>
17. H. Lu, L. Guo, G. Liu, S. Zhong, Progressive damage investigation of 2.5D woven composites under quasi-static tension. *Acta Mech.* **230**, 1323–1336 (2019). <https://doi.org/10.1007/s00707-017-2024-z>
18. M. Muñoz-Reja, L. Távara, V. Mantič, P. Cornetti, Crack onset and propagation at fibre–matrix elastic interfaces under biaxial loading using finite fracture mechanics. *Compos. A Appl. Sci. Manuf.* **82**, 267–278 (2016). <https://doi.org/10.1016/j.compositesa.2015.09.023>
19. M. Loos, Carbon nanotube reinforced composites: CNT Polymer Science and Technology. Elsevier. ISBN: 978-1-4557-3195-4 (2014).
20. R. Krueger, Virtual crack closure technique: History, approach, and applications. *Appl. Mech. Rev.* **57**(2), 109–143 (2004). <https://doi.org/10.1115/1.1595677>
21. M. Moslemim, M. Khoshrovan, Cohesive zone parameters selection for mode-I prediction of interfacial delamination. *J. Mech. Eng.* **61**(9), 507–516 (2015)
22. F. Shen, K.H. Lee, T.E. Tay, Modeling delamination growth in laminated composites. *Compos. Sci. Technol.* **61**(9), 1239–1251 (2001). [https://doi.org/10.1016/S0266-3538\(01\)00023-9](https://doi.org/10.1016/S0266-3538(01)00023-9)
23. T. Johannesson, P. Sjoblom, R. Seldon, The detailed structure of delamination fracture surfaces in graphite/epoxy laminates. *J. Mater. Sci.* **19**, 1171–1177 (1984). <https://doi.org/10.1007/BF01120026>
24. Z. Tian, S.R. Swanson, The fracture behavior of carbon/epoxy laminates containing internal cut fibers. *J. Compos. Mater.* **25**(11), 1427–1444 (1991). <https://doi.org/10.1177/002199839102501103>
25. S.S. Wang, Fracture mechanics for delamination problems in composite materials. *J. Compos. Mater.* **17**(3), 210–223 (1983). <https://doi.org/10.1177/002199838301700302>
26. J. Tao, C.T. Sun, Influence of ply orientation on delamination in composite laminates. *J. Compos. Mater.* **32**(21), 1933–1947 (1998). <https://doi.org/10.1177/002199839803202103>
27. D. Quan, J.L. Urdániz, A. Ivanković, Enhancing mode-I and mode-II fracture toughness of epoxy and carbon fibre reinforced epoxy composites using multi-walled carbon nanotubes. *Mater. Des.* **143**, 81–92 (2018). <https://doi.org/10.1016/j.matdes.2018.01.051>

Publisher's Note Springer Nature remains neutral with regard to jurisdictional claims in published maps and institutional affiliations.

Springer Nature or its licensor (e.g. a society or other partner) holds exclusive rights to this article under a publishing agreement with the author(s) or other rightsholder(s); author self-archiving of the accepted manuscript version of this article is solely governed by the terms of such publishing agreement and applicable law.